Three-dimensional Effects on Gap-Resonances in Twin-Hull Vessels in Time-Harmonic Vertical Oscillations

GIULIANO VERNENGO
Department of Electric, Electronic, Telecommunication Engineering and Naval Architecture (DITEN),
Polytechnic School of the University of Genova,
Via all'Opera Pia 11 A, 16145, Genova,
ITALY

Abstract: - Three-dimensional effects induced by dimensional ratios on the gap resonances happening in twin hull vessels oscillating in forced vertical motion have been analyzed. They can lead to relevant consequences, such as the amplification of the inner radiated waves or the generation of standing waves in between the demi-hulls, that can have a direct effect on the operating profile of the vessel. The response of twin hull vessels in waves can be strongly affected by these resonant phenomena. Also, some of these behaviors can be exploited in the framework of wave energy conversion systems. The present analysis is carried out by using an open-source, linear, Boundary Element Method (BEM), based on the Green function approach. Mathematical backgrounds of the added mass and damping coefficients computation for a floating body under harmonic vertical oscillation are provided as well as details of the numerical discretization used in the BEM. A panel mesh sensitivity study is carried out and the numerical prediction is validated by comparison against available experimental data, another CFD solution obtained by a high-fidelity viscous solver based on the open-source libraries Open-FOAM and approximate analytic formulations. The effect of the beam ratio and the length-to-beam ratio on the resonant phenomena has been analyzed. This has been achieved by systematic variations of the geometric dimensions of the hull, focusing on the trends of the hydrodynamic coefficients, the amplitude of the radiated waves, and the location of the resonant frequencies over the analyzed range.

Key-Words: - Gap resonance, Catamaran; Piston Mode, Wave Trapping, Sloshing frequencies, Boundary Element Method (BEM), Wave energy.

Received: March 19, 2023. Revised: February 9, 2024. Accepted: March 8, 2024. Published: May 2, 2024.

1 Introduction

Gap-induced resonances are extremely relevant to characterize the seakeeping response of floating structures, particularly at zero-forward speed. Such type of phenomena happen in the presence of a confined free water surface that can either be within the same body or between two adjacent bodies.

The first concern with the so-called moonpools, i.e. an opening in the hull giving access to the water creating a confined free surface. This is a typical design solution e.g. in drilling ships, ships for the installation of marine risers, and diving support vessels. The latter situation is instead typical of independent ships operating side-by-side such as e.g. barges, Floating Liquefied Natural Gas (LNG) Bunkering Terminal or Bunkering Shuttles serving LNG carriers, and connected twin hull surface piercing bodies such as multi-hull vessels like catamarans or Small Waterplane Area Twin Hulls (SWATHs).

Based on the exciting frequency of the motion and of the geometric features of the hulls different gap resonant phenomena can occur, as represented in Fig. 1.

The inner free surface in between the hulls shows two waving modes called piston and sloshing mode, respectively, happening at identifiable frequencies of oscillation. The first appears as a heavily amplified peak of the free surface oscillation concerning its normal behavior occurring at a single, specific, frequency. The sloshing mode generates a standing wave in the free surface in the gap, whose length depends on the oscillation frequency, that instead can be seen at different frequencies. The last resonance phenomenon, classified as trapping mode, results in the cancellation of the radiated wave outside of the gap. The correct prediction of the frequencies at which these phenomena will appear is of vital importance to correctly understand the possible limits of the operating profile of the many floating structures.

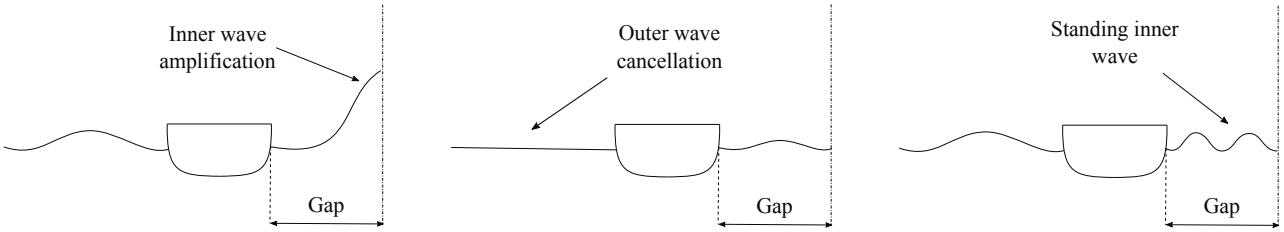

(a) *(b)* *(c)*

Fig. 1: Schematic representation of the most relevant resonant phenomena happening in multi-hull vessels in waves. A demi-hull is shown, and the symmetry plane of the vessel is indicated by a vertical dashed line. Left to right: Piston mode (a), Wave trapping (b), and Sloshing mode (c)

The occurrence of such a complex, non-linear, pressure-driven phenomenon can be captured in the context of potential theories, typically at the cost of overestimating the involved forces. This is mainly due to the absence of viscous effects and the lack of strongly non-linear free surface developments with possible fragmentation and wave breaking, a phenomenon that can be modeled by means e.g. of viscous Reynolds Averaged Navier Stokes (RANS), [1], [2] and by particle methods, [3], [4].

[5], developed an analytic solution to study the excitation of the free surface between two-dimensional sections. Potential flow-based methods have been widely used to analyze the piston mode resonance in rectangular barges with moonpools [6], in the presence of rigid ice sheets [7], side-by-side barges [8], [9], considering the effect of the finite water depth [10] and mooring lines, [11]. Two-dimensional studies on the piston and sloshing resonances have been carried out by [12] and by [13] accounting for coupled ship resonances. Recently, the resonance effects of moonpools with recesses have been studied by [14] and by [15]. In the framework of potential flow theories, suppression methods have been developed to deal with over-prediction of resonant phenomena such as the so-called rigid lid technique by [16], the flexible lid developed by [17], or the rigid damping method by [18]. These techniques have been applied to study resonances e.g. in side-by-side ships (see among the other [19], [20], [21], [22], [23]). Viscous effects in gap flows have been accounted for by coupling a Boundary Element Method (BEM) to a vortex tracking method [24] by using a Volume of Fluid method [25], by Spectral Wave Explicit Navier-Stokes approach [26] or by RANS computations [2], [27], [28], [29].

The sensitivity of gap resonance of catamaran hull at zero speed under forced, harmonic, and vertical oscillations concerning geometric parameters has been studied. Such a multi-hull configuration is of particular interest for many applications, including e.g. those related to wave energy conversion. The analysis is carried out in the framework of potential theory by using the open-source linear BEM, [30]. This solver has been used to study the performance of both single and arrays of Wave Energy Converters (WECs), [31], [32], [33] and it has been shown to provide results comparable to those obtained by other approaches [34]. This numerical method has also been used in the framework of multi-fidelity optimization of an unconventional SWATH with double-canted struts, [35].

The mathematical backgrounds and the numerical implementation of the BEM are briefly presented. A mesh coarsening study on the panel mesh density has been carried out before a preliminary validation of the hydrodynamic added mass and damping coefficients against available experimental data. The systematic study carried out by varying the dimensional ratios of the catamaran focuses on the identification of the gap resonant phenomenon, highlighting the effect of the selected geometric parameters on the occurrence and the type of resonance.

2 Mathematical Backgrounds of Frequency Domain Analysis of Oscillating Bodies

The problem of a body oscillating in forced motion at the free surface is described in the frequency domain within the framework of a linear potential theory. An ideal, incompressible, and irrotational fluid is assumed over a fluid domain Ω, leading to null viscosity $\nu = 0$, $\nabla \cdot \mathbf{V} = 0$ and null vorticity $\omega = \nabla \times \mathbf{V} = 0$, respectively, being $\mathbf{V}$ the fluid velocity. Thanks to these hypotheses, instead of using the Navier-Stokes equations, the problem could be solved by Euler and Bernoulli equations defining a velocity potential function Φ such that:

$$\boldsymbol{V} = \nabla\Phi = \boldsymbol{i}\frac{\partial \phi}{\partial x} + \boldsymbol{i}\frac{\partial \phi}{\partial x} + \boldsymbol{i}\frac{\partial \phi}{\partial x} \quad (1)$$

Such a velocity potential function satisfies the Laplace equation Eq. (3a) over Ω, plus several *ad-hoc* boundary conditions. Neumann-type boundary condition $\frac{\partial \Phi}{\partial n} = \boldsymbol{v}_{\mathrm{BK}} \cdot \mathbf{n}$ on the body surface S_B, stated that the normal velocity of the fluid vanishes at the body surface. Since a so-called radiation problem is under investigation, namely imposed body motions in calm water are considered, the term $\boldsymbol{v}_{\mathrm{BK}}$ represents the velocity of the rigid body induced by the k^{th} motion. Considering the specific problem of a body oscillating in a forced, vertical, sinusoidal motion $\eta_k(t) = \zeta_k \sin(\omega t)$, the potential function for the so-called radiation problem becomes $\Phi_k = \dot{\eta}_k(t)$, being $\dot{\eta}_k$ the time derivative of η_k. The conventional notation for ship motions is used so that k=3 identifies the heave (vertical) motion.

Considering the vertical harmonic oscillation $\eta_3 = \zeta_3 e^{i\omega_e t}$, being ζ_3 and ω their amplitude and frequency, respectively, the velocity $\dot{\eta}_3$ and the acceleration $\ddot{\eta}_3$ of the imposed motion are simply defined by derivation concerning time as in Eq. (2).

$$\begin{aligned} \dot{\eta}_3 &= i\omega\eta_3 = -i\omega\zeta_3 e^{-i\omega t} \\ \ddot{\eta}_3 &= -\omega^2\eta_3 = -\omega^2\zeta_3 e^{-i\omega t} \end{aligned} \tag{2}$$

So the rigid body vertical velocity induced by the imposed heave motion, projected onto the normal to the hull surface **n**, is $\boldsymbol{v}_{\mathrm{B3}} \cdot \mathbf{n} = i\omega n_3 e^{i\omega t}$. Being $\Phi = \phi e^{i\omega_e t}$, with ϕ the time independent potential function, the body boundary condition then holds as in Eq. (3b). A similar boundary condition representing null normal velocity at the horizontal bottom of the domain $z=z_{\mathrm{Bottom}}$, $\frac{\partial \phi_k}{\partial n} = 0$, is not necessarily for the proposed study since deep water case is investigated, $z_{Bottom} \to \infty$.

In addition, dynamic, $\frac{\partial \phi_k}{\partial t} + g\eta_{Wk} = 0$, and kinematic, $\frac{\partial \eta_{Wk}}{\partial t} - \frac{\partial \phi_k}{\partial z} = 0$, free surface boundary conditions, linearized at the undisturbed free surface level z=0, are imposed. In particular they are combined to exclude the term η_{Wk}, i.e. the radiated wave elevation, which is part of the solution of the problem, from the formulation itself to enable a linear solution of the system of equations, reaching the boundary condition at the free surface stated in Eq. (3c). A far-field, Sommerfeld-type, radiation condition ensuring that the potential nullify far away from the body, i.e. for an ideal distance $R \to \infty$, Eq. (3d) is also needed.

$$\begin{cases} \nabla^2\phi_k = 0 \quad \Omega \\ \dfrac{\partial \phi_k}{\partial n} = i\omega n_k \quad S_B \\ \omega^2\phi_k + \dfrac{g\partial \phi_k}{\partial z} = 0 \quad z = 0 \\ \sqrt{R}\left(\dfrac{\partial}{\partial n} - ik\right)\phi_k \to 0 \quad R \to \infty \end{cases} \tag{3}$$

The unknown potential function is found by solving a linear system of equations built on the above-mentioned boundary conditions. The time-independent j^{th} component of hydrodynamic radiation force induced by the k^{th} motion is then computed by integrating the dynamic pressure, excluding terms higher than first order from Bernoulli equation. For the forced heave motion, it results:

$$\frac{\boldsymbol{F}_{33}}{\zeta_3} = -\rho \int_{S_H} i\omega\phi_3 n_3 dS \tag{4}$$

Considering the model for rigid, floating body motions, hence introducing the three-dimensional added mass and damping coefficients A_{33} and B_{33}, respectively, i.e. the components of the hydrodynamic forces in phase with the acceleration and with the velocity, and accounting for Eq. (2), the time-independent, heave hydrodynamic force can be written as:

$$\boldsymbol{F}_{33} = \zeta_3(\omega^2 A_{33} - i\omega B_{33}) \tag{5}$$

The occurrence of the gap-resonances related phenomena can be identified by the analysis of the trends of these coefficients over a suitable range of oscillating frequencies.

2.1 Numerical Solution by Green Function based BEM

The hydrodynamic solution is found by using a three-dimensional BEM based on a Green function approach, suitable for offshore structures and floating bodies of generic shapes. According to [36], the first type Green function is written in the following form:

$$\begin{aligned} -4\pi G_\infty(r, Z, \omega) = \frac{1}{R} - \frac{1}{R_1} + G(r, Z, \omega) \\ + 2i\pi k_0 e^{k_0 Z} J_0(k_0 r) \end{aligned} \tag{6}$$

Being r the horizontal distance between the source point $P(x_P, y_P, z_P)$ and the field point $M(x_M, y_M, z_M)$, -Z the vertical distance between the image source point $P'(x_P, y_P, -z_P)$, mirrored concerning the mean free surface, and the field point M, R the distance between the source and field points and R_1 the distance between the image source

point and the field point. G_∞ is the deep water Green function and G represents the so-called free surface term. $J_0(k_0 r)$ is the 0^{th} order Bessel function of the first type and, from the deep-water dispersion relation, $k_0 = \frac{\omega^2}{g}$. *Nemoh* is based on a particular choice of the free surface term, [30], [37], which involves a finite integral of the complex exponential integral in the variable angle θ, defined as $cos\theta = -\frac{Z}{R_1}$, within the range $[-\frac{\pi}{2};\frac{\pi}{2}]$. The hull is represented by using N panels, either quadrilateral or triangular ones, arranged in an unstructured mesh. Considering that an unknown source $\sigma_i(P)$ is placed on the i^{th} panel, the discrete form of the induced velocity potential at a field point M can be resumed as:

$$\phi(P,M) = \frac{1}{4\pi}\sum_{i=1}^{N} G_\infty(P,M)\sigma_i(P) \qquad (7)$$

By using Eq. (7) and the boundary conditions of Eq. (3), a linear system of equations can be written in the unknown source strengths on each panel of the hull. Once the strength of the source distribution is found, all the other flow characteristics can be computed.

3 Benchmark Hull Shape

A round bilge catamaran hull has been selected as a reference shape for the present study, [38]. It is a cylindrical catamaran with a constant semi-circular cross-section as displayed in Fig. 2, where the characteristic dimensions of the hull, i.e. the demi-hulls separation 2b, the demi-hull beam 2a, the hull length L and the hull beam B, are shown too. The lateral positions of the buoys used for measuring the wave height both in between the demi-hulls and on the outer free surface are shown in the cross-section in Fig. 3. All the buoys are located at the longitudinal center of the hull. For such a hull, experimental values of the added mass and the damping coefficients are available.

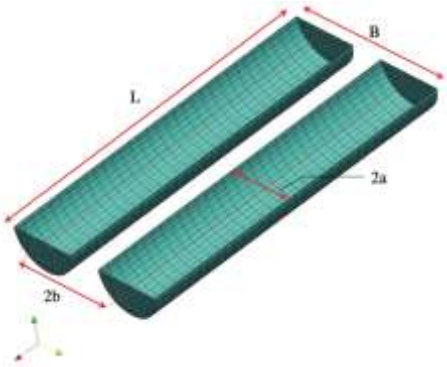

Fig. 2: Catamaran hull used for the systematic analysis of the resonant phenomena. Hull length, L, hull beam, B, demi-hull separation, 2b, and demi-hull beam, 2a, are highlighted

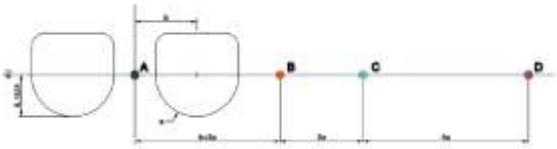

Fig. 3: Position of the probes used to measure the wave height

4 Results of the Analysis

A sensitivity analysis on the panel mesh density has been carried out and results are shown in the following Section 4.1. The validation of the numerical method by comparison against experimental data is presented in Section 4.2. Finally, results of the systematic variations of both the demi-hulls separation ratio $\frac{b}{a}$ and the length-to-beam ratio $\frac{L}{a}$ of the catamaran hull are presented in Section 4.3.

4.1 Panel Mesh Sensitivity

Effect of panel mesh density on the hydrodynamic coefficients has been investigated. The reference hull ratios are equal to L/a=10 and b/a=1.5. The three-panel meshes shown in Fig. 4 have been analyzed, namely a coarse mesh made of 400 panels, a medium-mesh made of 770, and a fine mesh made of 1200 elements. A structured panel mesh has been used for the whole hull surface but for the aft and forward closures where unstructured triangular panels have been used too. Aspect ratio equal to AR=1 has been used for the coarser mesh configuration while both the medium and fine meshes show rectangular panels with AR=0.5. The predicted heave-added mass and damping of the three meshes are compared in Fig. 5. They have been computed over the same range of oscillating

frequencies. Both coefficients are presented in non-dimensional form as $A_{33}/\rho\nabla$ and $B_{33}/\rho\nabla\omega$. Results from the medium and the fine meshes are equivalent. The coarser panel mesh shows slightly over-predicted peaks of both the added mass and the damping coefficients. Despite this difference, all the curves are in very good agreement, proving the robustness of the BEM prediction. In addition, since the computational time required by the three meshes almost doubles at each mesh density step, the medium-size mesh has been chosen for all the further computations.

Fig. 4: Three mesh configurations used for the sensitivity analysis on the catamaran hull with L/a=5 and b/a=1.5. Left to right: coarse, medium, and fine panel mesh

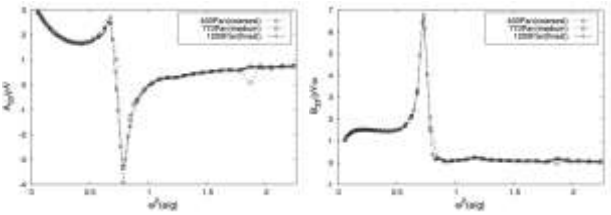

Fig. 5: Heave 3D added mass and damping coefficient computed by the BEM on the three mesh configurations used for the sensitivity analysis on the catamaran hull with L/a = 10 and b/a = 1.5

4.2 Validation of the BEM Prediction by Comparison Against Experimental Measurements

The experimental tests were carried out to reproduce 2D flow conditions by using two endplates at the catamaran aft and forward ends, [38]. The catamaran hull was located in the middle of the tank length, with the generating axis of the cylinders perpendicular to the sides of the tank so that the radiated waves could freely move alongside the tank itself.

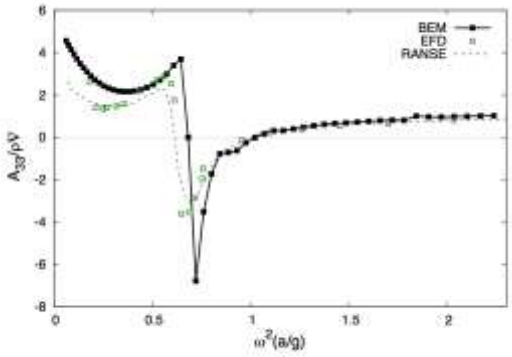

(a) b/a=1.5

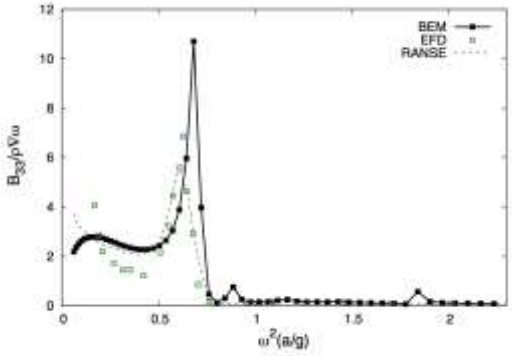

(b) b/a=1.5

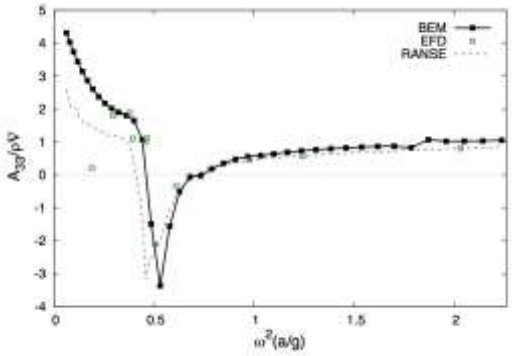

(c) b/a=2.0

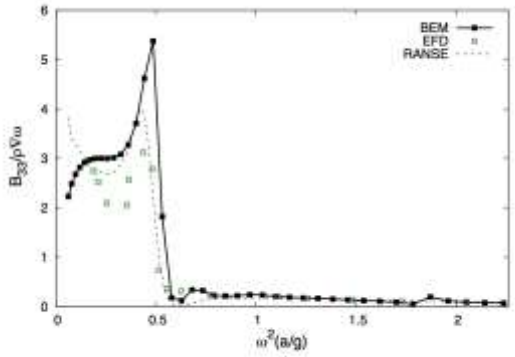

(d) b/a=2.0

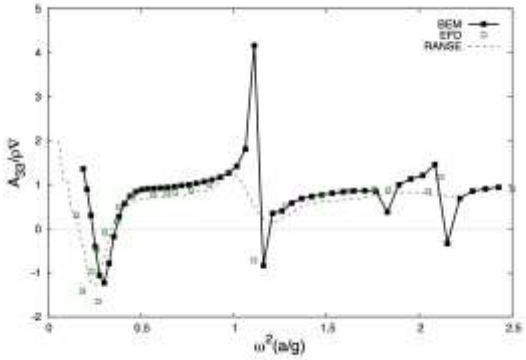

(e) b/a=4.0

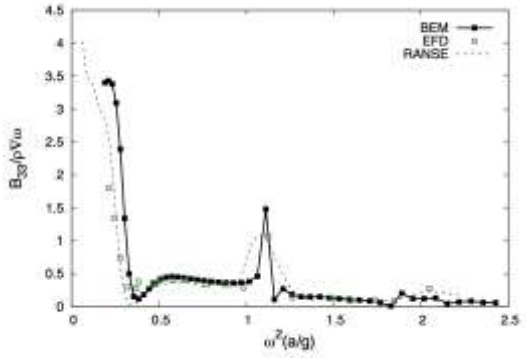

(f) b/a=4.0

Fig. 6: Non-dimensional 3D heave added mass and damping coefficients for the catamaran hull having B/L = 18. Top to bottom: b/a = 1.5; 2.0; 4.0. Left column: added mass coefficients. Right column: damping coefficients. BEM (filled black squares), RANSE (dashed line), and EFD (empty green squares) results are shown

Fig. 6 compares the experimental and the numerical results for the hull with the highest length-to-beam ratio, namely L/a=18. This is the higher aspect ratio configuration then reducing as much as possible the three-dimensional effects. Three beam-to-length ratios have been analyzed, corresponding to b/a=1.5; 2.0; and 4.0, respectively. Results obtained by using a high-fidelity, viscous, 2D RANS solver based on openFOAM libraries, [39] are shown too. Such a RANS approach has been validated in several seakeeping-related problems involving both oscillating SWATH sections, [40] and ship motion prediction, [41].

The experimental measurements and the numerical predictions are in good agreement over the entire range of analyzed frequencies for both the added mass and damping coefficients, respectively. The location of the peaks of the hydrodynamic coefficients is well predicted. However, either the experimental measurements or the RANS predictions show lower values of these peaks of the responses due to the lack of any viscous correction in the BEM results.

Considering the inversion of the trends added mass coefficients crossing the horizontal axis, the piston mode gap resonance is experienced by all three designs. This phenomenon happens at decreasing frequencies as the separation increases, ranging from $\frac{\omega^2 a}{g} = 0.6$ for b/a=1.5 to $\frac{\omega^2 a}{g} = 0.3$ for b/a=4.0. At the piston mode resonance, the damping coefficient is maximum meaning that the energy dissipated by the radiated wave is the highest. Close to the piston mode gap resonance, at a slightly higher frequency the hull experiences the so-called wave trapping. This phenomenon appears as a cancellation of the outer radiated wave and can then be identified by the nullification of the damping coefficient. Consistently, the lower trapping frequency is found at the higher hull separation.

At the higher separation ratio, i.e. b/a=4.0, two sloshing frequencies are discovered by analyzing the trend of the added mass coefficient. Numerical results obtained by using the BEM are consistent with those obtained from Eq. (8) defining a standing wave derived from the dispersion relation for infinite depth.

$$\omega_{sloshing} = \sqrt{\frac{n\pi g}{b-a}} \tag{8}$$

According to this simplified formulation, the sloshing frequencies should be $\omega_1 = 1.04$ and $\omega_2 = 2.09$, for n=1 and n=2, respectively.

The other sudden variation of the response found by the BEM at $\frac{\omega^2 a}{g} = 1.72$ is referred to an irregular frequency. This is a numerical issue of the BEM that of course is not seen neither in the experiments nor by the RANSE. This is a well-known drawback of the Green function approach first highlighted by [42], [43]. It has then been described e.g. by [44] in analogy to the sloshing that happens on the fictitious free surface contained inside the hull. For the proposed study, it is unnecessary to use irregular frequency suppression methods, but it is enough to identify this numerical behavior of the BEM.

[45], provides an approximate formulation for irregular frequencies of a simple rectangular pontoon only based on its length and beam, L and B, respectively, and on the depth T. By using Eq. (9) on the single demi-hull of the catamaran the first irregular frequency, corresponding to the variation of the trend of the coefficients, is found.

$$\omega_{irregular} = \sqrt{\frac{\frac{\pi g}{L}\sqrt{\frac{L^2+B^2}{B^2}}}{\tanh\left(\frac{\pi T}{L}\sqrt{\frac{L^2+B^2}{B^2}}\right)}} \tag{9}$$

Specific features of the radiated wave patterns are triggered at each gap resonance identified by analyzing the trends of the hydrodynamic coefficients. However, there have been no available data to verify the prediction of the radiated waves. Then, an approximate theoretical formulation has been used to carry out such a validation on the radiated waves. Such a theoretical approach is rigorously valid in the framework of a linear theory, neglecting the second-order interactions between the hull surface and the waves, meaning that the hull would have vertical sides, i.e. a rectangular section, and that a mean wet hull surface can be considered. Assuming that (a) the potential-flow damping is related to the outgoing waves, (b) the energy is carried out of the hull by the outgoing waves, (c) the BEM can capture the generation of such waves, the work of the damping force can be equated to the power associated to the radiated waves. Considering a hull heaving at a given frequency ω, the work exerted by the damping forces over an oscillation period $T = \frac{2\pi}{\omega}$ can be written as in Eq. (10):

$$\begin{aligned}\bar{L}_{B_{33}} &= \frac{1}{T}\int_0^T B_{33}\dot{\eta}_3 d\eta_3 \\ &= \frac{1}{2\pi} B_{33}\zeta_3^2\omega_3 \int_0^{2\pi/\omega} \sin^2(\omega t)\, dt \\ &= \frac{1}{2} B_{33}\zeta_3^2\omega^2\end{aligned} \tag{10}$$

Being ζ_3 the amplitude of the heaving motion $\eta_3 = \zeta_3 \cos(\omega t)$.

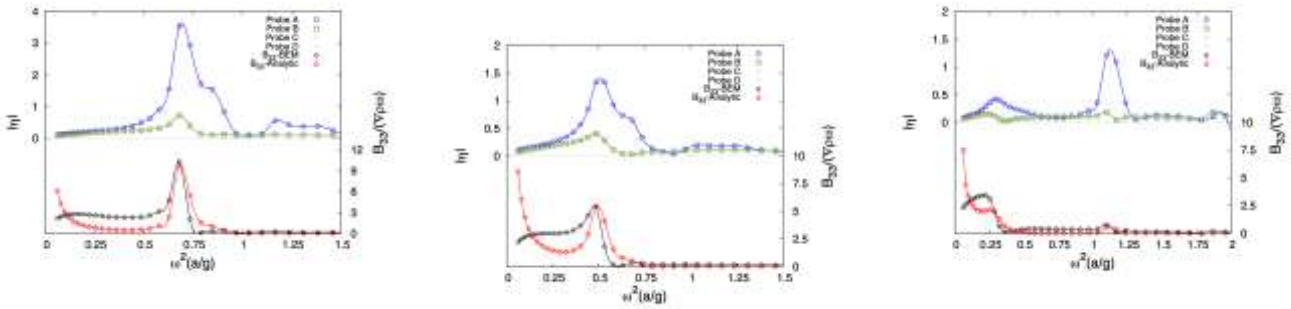

Fig. 7: Comparison of the damping coefficient B_{33} computed by using the BEM (black curve) and the analytic formulation (red curve) based on the radiated waves, shown on the top side of each sub-figure

The power of the radiated outgoing waves over an oscillation period can be written based on the mean energy flux $\frac{d\bar{E}}{dt} = c_g \bar{E}$, being $c_g = \frac{g}{\omega}$ the group celerity, as in the following Eq. (11):

$$\bar{L}_{Wave} = \frac{d\bar{E}}{dt} T = 2\left[\frac{1}{2}\rho g\left(a_{in}^2 + a_{out}^2\right)c_g\right]T = \frac{2\rho g^2 \pi}{\omega^2}\left(a_{in}^2 + a_{out}^2\right) \quad (11)$$

where a_{in} and a_{out} are the amplitude of the radiated waves at the inner free surface and at the outer free surface. These waves are here assumed to be cylindrical. The multiplying factor 2 has been left out of the square brackets to highlight that this energetic contribution needs to be doubled due to the twin-hull. By equating Eq. (10) to Eq. (11) and considering $\zeta_3 = 1$, an approximate, analytic formulation for the (potential) heave damping coefficient can be found as:

$$B_{33}^* = \frac{4\rho g^2 \pi}{\omega^4}\left(a_{in}^2 + a_{out}^2\right) \quad (12)$$

Fig. 7 displays the amplification of the inner wave for the design with b/a=1.5, measured at the four buoys (Fig. 3), for an harmonic oscillation corresponding to the piston mode resonant frequency. The wave height reaches a maximum value of $\eta_A \cong 3.69$ at the inner buoy A, that is much higher than the average value of $\eta_A \cong 0.53$ or than the amplitude reached at the outer free surface where $\eta_{MAX} \cong 0.78$. The amplitude of the radiated wave pattern is higher at the inner free surface close to the center of the hulls while decaying towards the aft and forward ends of the catamaran due to the three-dimensional effects, as shown in Fig. 7. The inner free surface elevation is far higher than that of the outer free surface at this first gap resonance frequency.

Eq. (13) has been proposed to find the piston mode frequencies of a moonpool [6]:

$$\omega_{piston} = \sqrt{\frac{g}{h + \frac{B}{\pi}\left(\frac{3}{2}\ln\left(\frac{H}{2b}\right)\right)}} \quad (13)$$

Being b the beam of the moonpool, corresponding in this case to the distance between the two demi-hulls, h the depth and H the beam of the whole body, corresponding to the beam of the whole catamaran. As further verification, Table 1 reports the comparison between the piston mode frequencies computed by using Eq. (13) and those predicted by the BEM. An acceptable agreement is obtained. A general over-prediction of the piston mode frequencies is experienced by the BEM that decreases as the hull separations increase. The maximum percentage difference $\Delta\epsilon = 14.2\%$ is found for the lower transverse hull separation.

Table 1. Non-dimensional piston mode frequencies ω2a/g for the hull having L/B = 18.

b/a	Eq. (13)	BEM	$\Delta\epsilon$
1.5	0.709	0.81	14.2%
2.0	0.614	0.68	10.2%
4.0	0.455	0.46	1.10%

Fig. 7 and Fig. 8 display an example of wave elevation and wave pattern, respectively, at the wave trapping frequency for the hull with b/a=2.0. At such oscillation frequency the minimum amplitude of the external radiated waves, that are almost completely canceled, is reached. This is consistent with the trend of the damping coefficient that is very close to zero at $\omega_{trapping}$. In fact, B_{33} does not depend on the viscous effects since it is a force coefficient derived in the framework of a potential theory. It is depending on the energy dissipated by the generation of the radiated waves. If no waves are generated, no (potential-flow) damping is created, and *vice versa*. The cancellation is related to the outer wave field that is the most responsible for the energy dissipation, then contributing to a great extent to the damping coefficient. The small values of the B_{33} coefficient are related to both the inner wave, which is anyway present, and again to the three-dimensional characteristic of the wave pattern.

Effects of oscillations at the sloshing frequencies are highlighted in Fig. 7 for the hull configuration with b/a=4.0. This gap resonance occurs at relatively higher frequencies compared to the other two previously described phenomena. This means that it generally happens for faster oscillations. Local amplification of the inner wave is shown in Fig. 8 at the two discovered sloshing frequencies. The characteristics of the wave pattern in between the two hulls resemble those of standing waves whose frequencies are proportional to the oscillation frequency of the body. The wave elevation of the free surface is shown in Fig. 8 for the first and the second sloshing frequencies, respectively. At the lower sloshing frequency, the inner wave pattern shows three wave crests in the transverse direction while five crests are identified at the higher sloshing frequency. Consistently with $\omega_{sloshing-1} < \omega_{sloshing-2}$, this means that longer waves are generated in the first case while shorter waves are created in the second one.

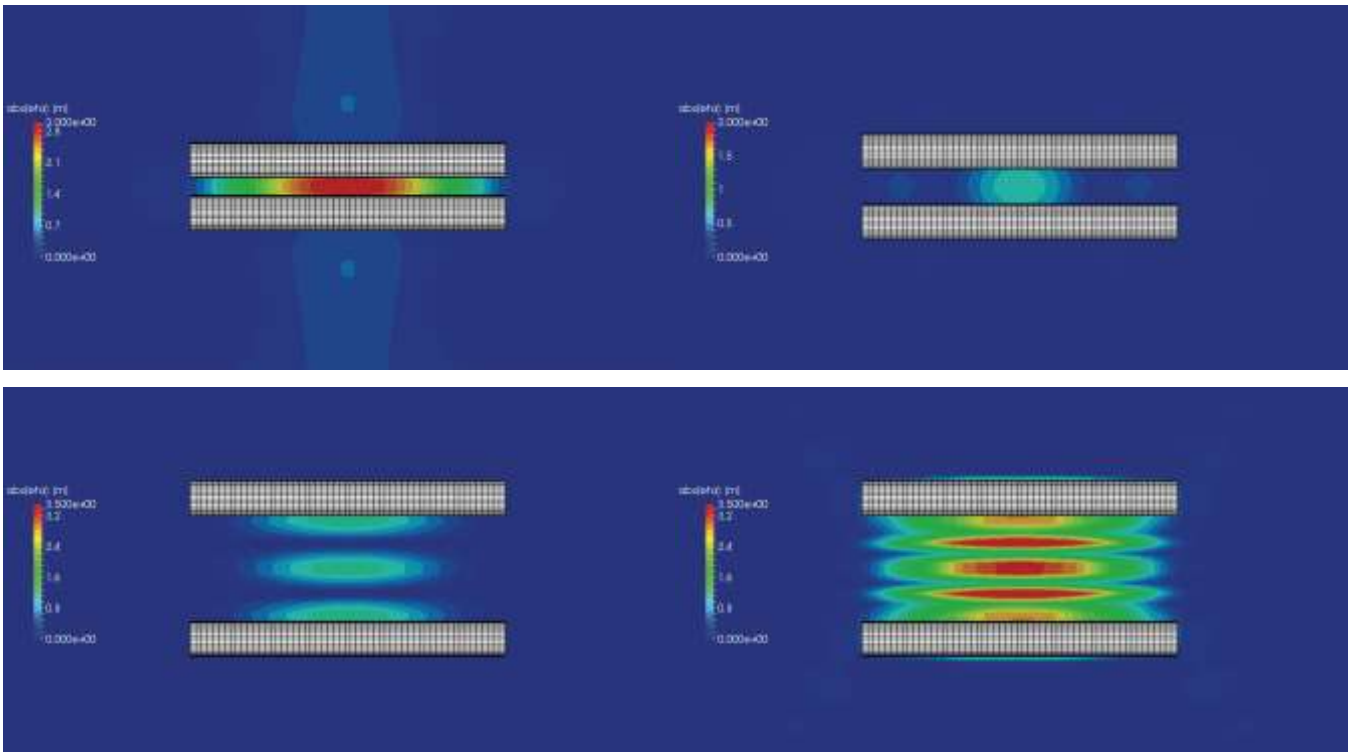

Fig. 8: Top view of the real part of the three-dimensional radiated wave patterns at different separation ratios. Top left, clockwise: piston mode, trapping mode, 1st sloshing mode, 2nd sloshing mode

4.3 Sensitivity Analysis of the Effects of the Hull Geometric Ratios

A systematic variation of two relevant geometric ratios of the catamaran have been carried out to investigate their effect on the occurrence of the gap resonances. A separation ratio and a slenderness ratio, b/a and L/a, respectively, have been considered. The first is defined as the ratio between the demi-hull separation distance and the beam of the demi-hull. The latter is defined as the ratio between the hull length and the beam of the demi-hull. Nine combinations have been accounted for, by using the following values:

$$\frac{b}{a} = [1.5; 2.0; 4.0]$$
$$\frac{L}{B} = [10; 14; 18] \quad (14)$$

Each hull design is then identified by a couple of values of (b/a; L/B). The added mass and damping coefficients for each design undergoing forced heave motion have been computed by the BEM over a range of oscillation frequencies corresponding to $\frac{\omega^2 a}{g} = [0.60; 2.25]$. To focus on the trends of these responses, the results have been interpolated over a continuous domain. In particular, a Gaussian Process regression-based fitting method (see for instance [45], [46]) has been used to create the response surfaces corresponding to A_{33} and B_{33} at a given L/a ratio. This class of methods has been recently used e.g. in the context of single and multi-fidelity optimization [35], [47], [48], [49] and big data regression, [50] and it is here applied to reveal the trends of the hydrodynamic coefficients to concerning changes of the geometric ratios.

Fig. 9 highlights a trend on both the added masses and damping that is common to all three ratios L/a. The first negative peak of $A_{33}/\rho\nabla$, close to the piston mode gap resonance, is decreased and shifted to lower frequencies as the separation ratio increases. The maximum value of such peaks of the added mass increases as the length-to-beam ratio increases. This has a twofold meaning. On a side, the effect of the forces that are synchronized with the acceleration of the body becomes less relevant increasing the separation between the demi-hulls, and as expected, such an effect is strongly decreased by the three-dimensional effects, i.e. for the maximum L/a.

Considering again the trends of the added mass coefficient, two sloshing mode gap resonances are identified in the upper half of the range of the separation ratio. The maximum variation of $A_{33}/\rho\nabla$ due to this gap resonance corresponds to the second sloshing mode frequency at the intermediate length-to-beam ratio L/a=14.

All the peaks of the responses, except that of the second sloshing mode frequency, are increased at the highest L/a, especially those of $B_{33}/\rho\nabla\omega$. This means that the gap resonances happen at the same oscillation frequency, regardless the value of the slenderness ratio but with a different amplitude. The b/a ratio instead is more responsible for the type of gap resonance, since the piston mode resonance is revealed in the lower half of its range while the sloshing mode resonance appears for higher values. Consistently with the results obtained by other authors [6], the piston mode resonance frequency predicted by the BEM is inversely proportional to the distance between the demi-hulls, as displayed in Fig. 10. It slightly decreases as the length-to-beam ratio increases. The inner wave amplitude is heavily amplified, up to four times the amplitude of the oscillation for [b/a=1.5; L/a=18]. So, as expected, the piston mode is greatly affected by the distance between the demi-hulls. As regards the wave trapping phenomenon, there are no simplified formulations based e.g. on dimensional ratios of the body.

The wave trapping frequency decreases as the gap of the hull increases being $\frac{\omega^2_{Trapping}a}{g} = [0.802;\ 0.628;\ 0.384]$ for b/a=[1.5; 2.0; 4.0], respectively. Since this phenomenon strongly depends on non-linear effects, this trend is possibly due to the different interactions between the demi-hulls. Moreover, it seems that this cancellation of the external radiated wave could occur at several frequencies in the case of the larger separation b/a=4.0 for which $B_{33}/\rho\nabla\omega$ tends to zero at least three times, for $\frac{\omega^2 a}{g} = [0.38; 1.16; 2.15]$. This last result however should be further verified by using a fully viscous, non-linear, method.

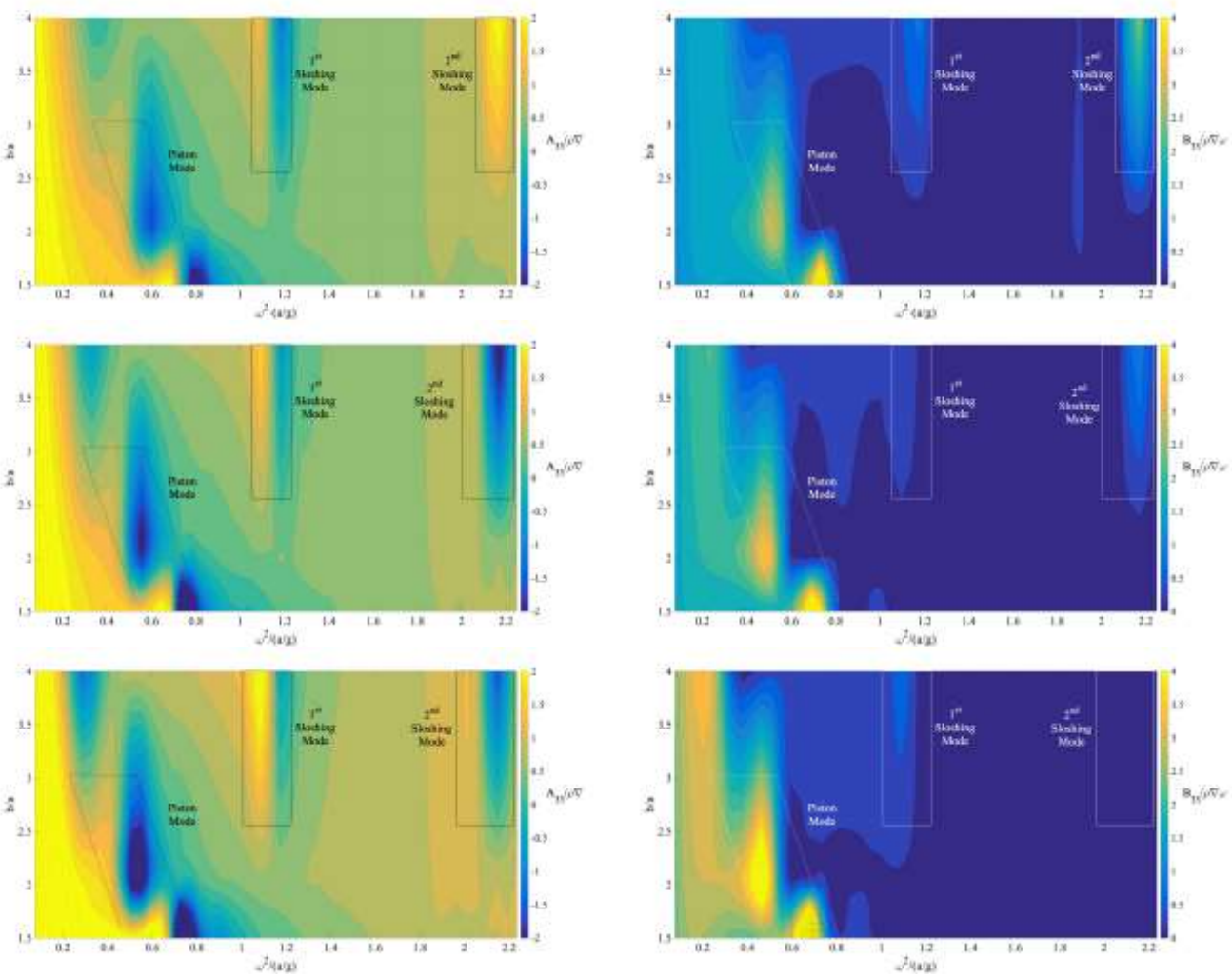

Fig. 9: Non-dimensional 3D heave added mass and damping coefficients in the continuous range b/a = [1.5; 4.0]. Top to bottom: L/a = 10; 14; 18. Left column: non-dimensional added mass coefficient. Right column: non-dimensional damping coefficient

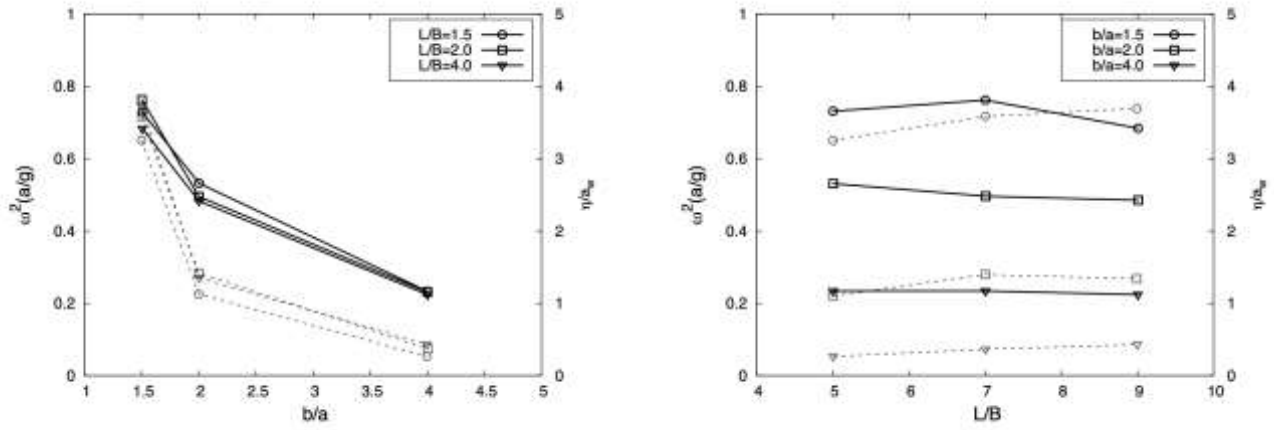

Fig. 10: Non-dimensional piston mode frequency (solid lines, left y axis) and non-dimensional inner wave amplitude at Probe A (dashed lines, right y axis) as function of b/a and L/a ratios

5 Conclusion

A numerical analysis of the gap resonances happening in twin hull vessels undergoing forced, harmonic, vertical motion at zero forward speed has been proposed. An open-source linear Boundary Element Method has been applied to this aim. The mathematical framework and the numerical approach used to predict these resonant phenomena have been described. A preliminary sensitivity analysis of the numerical prediction concerning the panel mesh density has been carried out finding the best trade-off between accuracy and computational time. The numerical method has then been validated by comparison against available experimental towing tank results. A satisfactory agreement has been found over a wide range of oscillation frequencies between the BEM prediction, the experimental results, and previous results from the high-fidelity viscous RANSE solver.

The influence of the demi-hull separation ratio and the hull length-to-beam ratio have been investigated by systematic numerical analysis. Nine hull configurations have been studied in terms of added mass and damping coefficients focusing on the occurrence of significant gap-resonances. Both the piston mode and the sloshing resonance frequencies predicted by the BEM are like those provided by approximate formulations available in the literature, proving that the method can recognize such a phenomenon. Wave trapping frequencies have been identified by the trends of the hydrodynamic coefficients. Such a resonant phenomenon happens at lower frequencies as the gap between the demi-hulls increases. The obtained results highlighted a general major effect of the separation ratio of the hull concerning the slenderness ratio. This, in conclusion, means that the three-dimensional effects at the afterward and forward ends of the hull are less relevant than the transverse size of the gap on the occurrence of these resonant phenomena.

That information might be of particular relevance in at least two cases: on one side, if seakeeping is concerned, to avoid specific wave frequencies to minimize e.g. unwanted wave behaviors in between the demi-hulls and, on the opposite side, if wave energy devices want to be created based on twin hull configuration to capture the maximum possible wave elevation of the piston mode.

References:

[1] Bonfiglio, L.; Brizzolara, S.; Chryssostomidis, C. Added mass and damping of oscillating bodies: a fully viscous numerical approach. *Recent Advances in Fluid Mechanics, Heat & Mass Transfer and Biology*, 2011, pp. 210–215, Corpus ID: 174775457.

[2] Bonfiglio, L.; Brizzolara, S. Amplitude Induced Nonlinearity in Piston Mode Resonant Flow: A Fully Viscous Numerical Analysis. *Journal of Offshore Mechanics and Arctic Engineering*, 2018, 140, 011101.

[3] Roselli, R.A.R.; Vernengo, G.; Brizzolara, S.; Guercio, R. SPH simulation of periodic wave breaking in the surf zone - A detailed fluid dynamic validation. *Ocean Engineering*, 2019, 176, 20-30,

https://doi.org/https://doi.org/10.1016/j.oceaneng.2019.02.013.

[4] Vineesh, P.; Sriram, V. Numerical investigation of wave interaction with two closely spaced floating boxes using particle method. *Ocean Engineering*, 2023, 268, 113465.

[5] McIver, P.; McIver, M.; Zhang, J. Excitation of trapped water waves by the forced motion of structures. *Journal of Fluid Mechanics*, 2003, 494, 141–162.

[6] Molin, B. On the piston and sloshing modes in moonpools. *Journal of Fluid Mechanics*, 2001, 430, 27–50.

[7] Molin, B.; Remy, F.; Kimmoun, O.; Stassen, Y. Experimental study of the wave propagation and decay in a channel through a rigid ice-sheet. *Applied ocean research*, 2002, 24, 247–260.

[8] Molin, B.; Remy, F.; Camhi, A.; Ledoux, A. Experimental and numerical study of the gap resonances in-between two rectangular barges. *In Proceedings of the 13th Congress of the International Maritime Association of the Mediterranean (IMAM 2009)*, Instanbul, Turkey, 2009, pp. 12–15.

[9] Zhao, S.; Gao, Z.; Meng, X.; Li, H. Multibody coupled dynamic response analysis of a dual barge float-over operation system with motion compensation equipment under a passive operational mode. *Ocean Engineering*, 2023, 269, 113499.

[10] Molin, B.; Zhang, X.; Huang, H.; Remy, F. On natural modes in moonpools and gaps in finite depth. *Journal of Fluid Mechanics*, 2018, 840, 530–554.

[11] Chen, M.; Guo, H.; Wang, R.; Tao, R.; Cheng, N. Effects of gap resonance on the hydrodynamics and dynamics of a multi-module floating system with narrow gaps. *Journal of Marine Science and Engineering*, 2021, 9, 1256.

[12] Faltinsen, O.M.; Rognebakke, O.F.; Timokha, A.N. Two-dimensional resonant piston-like sloshing in a moonpool. *Journal of Fluid Mechanics,* 2007, 575, 359–397.

[13] Kristiansen, T.; Faltinsen, O. A two-dimensional numerical and experimental study of resonant coupled ship and piston-mode motion. *Applied Ocean Research*, 2010, 32, 158–176.

[14] Molin, B. On natural modes in moonpools with recesses. *Applied Ocean Research*, 2017, 67, 1–8.

[15] Newman, J. Resonant response of a moonpool with a recess. *Applied Ocean Research*, 2018, 76, 98–109.

[16] Huijsmans, R.; Pinkster, J.; De Wilde, J. J. Diffraction and radiation of waves around side-by-side moored vessels. *In Proceedings of the The Eleventh International Offshore and Polar Engineering Conference*. International Society of Offshore and Polar Engineers, Szczecin, Poland, 2001.

[17] Newman, J. Progress in wave load computations on offshore structures. *In Proceedings of the 23rd International Conference Offshore Mechanics & Arctic Engineering*, Vancouver, Canada, June, 2004, pp. 20–25.

[18] Chen, X.B. Hydrodynamic analysis for offshore LNG terminals. *In Proceedings of the 2nd International Workshop on Applied Offshore Hydrodynamics*, Rio de Janeiro, 2005.

[19] Buchner, B.; Loots, G.; Forristall, G.; Van Iperen, E. J. Hydrodynamic aspects of gravity based structures in shallow water. *In Proceedings of the Offshore Technology Conference*. Houston, Texas, USA, 2004.

[20] Lewandowski, E.M. Multi-vessel seakeeping computations with linear potential theory. *Ocean Engineering*, 2008, 35, 1121–1131.

[21] Hong, D.; Hong, S.; Nam, B.; Hong, S. Comparative numerical study of repulsive drift forces and gap resonances between two vessels floating side-by-side in proximity in head seas using a discontinuous HOBEM and a constant BEM with boundary matching formulation. *Ocean Engineering*, 2013, 72, 331–343.

[22] Watai, R.; Dinoi, P.; Ruggeri, F.; Souto-Iglesias, A.; Simos, A. Rankine time-domain method with application to side-by-side gap flow modeling. *Applied Ocean Research,* 2015, 50, 69–90.

[23] Zou, M.; Chen, M.; Zhu, L.; Li, L.; Zhao, W. A constant parameter time domain model for dynamic modelling of multi-body system with strong hydrodynamic interactions. *Ocean Engineering*, 2023, 268, 113376.

[24] Kristiansen, T.; Faltinsen, O. Application of a vortex tracking method to the piston-like behaviour in a semi-entrained vertical gap. *Applied Ocean Research*, 2008, 30, 1–16.

[25] Kristiansen, T.; Faltinsen, O.M. Gap resonance analyzed by a new domain-decomposition method combining potential

and viscous flow DRAFT. *Applied Ocean Research*, 2012, 34, 198–208.

[26] Elie, B.; Reliquet, G.; Guillerm, P.E.; Thilleul, O.; Ferrant, P.; Gentaz, L.; Ledoux, A. Simulation of the gap resonance between two rectangular barges in regular waves by a free surface viscous flow solver. *In Proceedings of the 32nd International Conference on Ocean, Offshore and Arctic Engineering*. American Society of Mechanical Engineers (ASME), Nantes, France, 2013, pp. V005T06A083–V005T06A083.

[27] Chen, L.; Cao, X.; Sun, S.; Cui, J. The effect of draft ratio of side-by-side barges on fluid oscillation in narrow gap. *Journal of Marine Science and Engineering*, 2020, 8, 694.

[28] Sun, J.Y.; Sun, S.L.; Sun, S.Z.; Ren, H.L. The impact of piston and sloshing motions on added resistance from moonpool configurations. *Ocean Engineering*, 2023, 267, 113179.

[29] Gao, J.; He, Z.; Huang, X.; Liu, Q.; Zang, J.; Wang, G. Effects of free heave motion on wave resonance inside a narrow gap between two boxes under wave actions. *Ocean Engineering*, 2021, 224, 108753.

[30] Babarit, A.; Delhommeau, G. Theoretical and numerical aspects of the open source BEM solver NEMOH. *In Proceedings of the 11th European Wave and Tidal Energy Conference (EWTEC2015)*, Nantes, France, 2015.

[31] Schmitt, P.; Asmuth, H.; Elsäßer, B. Optimising power take-off of an oscillating wave surge converter using high fidelity numerical simulations. *International journal of marine energy*, 2016, 16, 196–208.

[32] Babarit, A.; Singh, J.; Mélis, C.; Wattez, A.; Jean, P. A linear numerical model for analysing the hydroelastic response of a flexible electroactive wave energy converter. *Journal of Fluids and Structures*, 2017, 74, 356–384.

[33] Flavià, F.F.; Mcnatt, C.; Rongè e, F.; Babarit, A.; Clé ent, A.H. A numerical tool for the frequency domain simulation of large arrays of identical floating bodies in waves. *Ocean Engineering*, 2018, 148, 299–311.

[34] Penalba, M.; Kelly, T.; Ringwood, J.V. *Using NEMOH for modelling wave energy converters: a comparative study with WAMIT*. Centre for Ocean Energy Research (COER), Maynooth University, Co. Kildare, Ireland 2017.

[35] Bonfiglio, L.; Perdikaris, P.; Vernengo, G.; de Medeiros, J.S.; Karniadakis, G. Improving SWATH Seakeeping Performance using Multi-Fidelity Gaussian Process and Bayesian Optimization. *Journal of Ship Research*, 2018, 62, 223–240.

[36] Xie, C.; Choi, Y.; Rongè e, F.; Clé ent, A.H.; Delhommeau, G.; Babarit, A. Comparison of existing methods for the calculation of the infinite water depth free-surface Green function for the wave–structure interaction problem. *Applied Ocean Research* 2018, 81, 150–163, https://doi.org/10.1016/j.apor.2018.10.007.

[37] Delhommeau, G. Seakeeping codes aquadyn and aquaplus. *19th WEGEMT School Numerical Simulation of Hydrodynamics: Ships and Offshore Structures*, Nantes, France, 1993.

[38] Lee, C.; Jones, H.; Bedel, J. *Added mass and damping coefficients of heaving twin cylinders in a free surface*. Technical report, DTIC Document, 1971.

[39] Bonfiglio, L.; Brizzolara, S. Unsteady Viscous Flow with Non Linear Free Surface around Oscillating SWATH Ship Sections. *WSEAS Transactions on Fluid Mechanics*, 2014, vol.9, pp.49–57.

[40] Bonfiglio, L.; Vernengo, G.; Brizzolara, S.; Bruzzone, D. A hybrid RANSE–strip theory method for prediction of ship motions. *In Proceedings of the Maritime Technology and Engineering III: Proceedings of the 3rd International Conference on Maritime Technology and Engineering* (MARTECH 2016, Lisbon, Portugal, 4-6 July 2016). CRC Press, 2016, p. 241.

[41] John, F. On the motion of floating bodies II. Simple harmonic motions. *Communications on pure and applied mathematics*, 1950, 3, 45–101.

[42] Frank, W. Oscillation of cylinders in or below the free surface of deep fluids. *Technical report*, DTIC Document, 1967.

[43] Liapis, S. A method for suppressing the irregular frequencies from integral equations in water wave-structure. Interaction problems. *Computational mechanics*, 1993, 12, 59–68.

[44] Det Norske Veritas, D.N.V. *Modelling and analysis of marine operations*. DNV-RP-H103, Offshore Standard 2011.

[45] Rasmussen, C.E.; Williams, C. *Gaussian Processes for Machine Learning*, Cambridge, 2006.

[46] Forrester, A.; Sobester, A.; Keane, A. *Engineering design via surrogate modelling: a practical guide*; John Wiley & Sons, 2008.
[47] Perdikaris, P.; Karniadakis, G.E. Model inversion via multi-fidelity Bayesian optimization: a new paradigm for parameter estimation in haemodynamics, and beyond. *Journal of The Royal Society Interface*, 2016, 13, 20151107. 45
[48] Coppedè, A.; Gaggero, S.; Vernengo, G.; Villa, D. Hydrodynamic shape optimization by high fidelity CFD solver and Gaussian process based response surface method. *Applied Ocean Research*, 2019, 90, 101841.
[49] Gaggero, S.; Coppede, A.; Villa, D.; Vernengo, G.; Bonfiglio, L. A data-driven probabilistic learning approach for the prediction of controllable pitch propellers performance. *In Proceedings of the Proceedings of the VIII International Conference on Computational Methods in Marine Engineering (MARINE 2019)*, 2019, pp. 1–12, Gothenburg, Sweden, 13–15 May 2019.
[50] Raissi, M. *Parametric Gaussian process regression for big data*. arXiv preprint arXiv:1704.03144 2017.

Contribution of Individual Authors to the Creation of a Scientific Article (Ghostwriting Policy)

Giuliano Vernengo carried out the simulation, analysed the results, wrote and reviewed the manuscript.

Sources of Funding for Research Presented in a Scientific Article or Scientific Article Itself

No funding was received for conducting this study.

Conflict of Interest

The author has no conflicts of interest to declare.